

Electrochemical properties of core-shell TiC–TiO₂ nanoparticle films immobilized at ITO electrode surfaces

Susan J. Stott,^a Roger J. Mortimer,^a Sandie E. Dann,^a Munetaka Oyama^b and Frank Marken^{*c}

Received 19th July 2006, Accepted 3rd October 2006

First published as an Advance Article on the web 26th October 2006

DOI: 10.1039/b610391j

Titanium carbide (TiC) nanoparticles are readily deposited onto tin-doped indium oxide (ITO) electrodes in the form of thin porous films. The nanoparticle deposits are electrically highly conducting and electrochemically active. In aqueous media (at pH 7) and at applied potentials positive of 0.3 V vs. SCE partial anodic surface oxidation and formation (at least in part) of novel core-shell TiC–TiO₂ nanoparticles is observed. Significant thermal oxidation of TiC nanoparticles by heating in air occurs at a temperature of 250 °C and leads first to core-shell TiC–TiO₂ nanoparticles, next at ca. 350 °C to TiO₂ (anatase), and finally at temperatures higher than 750 °C to TiO₂ (rutile). Electrochemically and thermally partially oxidized TiC nanoparticles still remain very active and for some redox systems electrocatalytically active. Scanning and transmission electron microscopy (SEM and TEM), temperature dependent XRD, quartz crystal microbalance, and voltammetric measurements are reported. The electrocatalytic properties of the core-shell TiC–TiO₂ nanoparticulate films are surveyed for the oxidation of hydroquinone, ascorbic acid, and dopamine in aqueous buffer media. In TiC–TiO₂ core-shell nanoparticle films TiO₂ surface reactivity can be combined with TiC conductivity.

1. Introduction

Titanium carbide, TiC, is a typical early transition metal carbide with many desirable materials properties such as extreme hardness, high electrical conductivity, and a high melting point, ideal for applications as wear resistant coatings.¹ Further advantageous properties include catalytic activity² and electrocatalytic activity,³ which are highly beneficial for applications as a potential electrode or sensor material. Very little is known about the electrochemical properties of TiC materials and there are currently no studies reporting the properties of TiC nanomaterials. However, in sharp contrast, a lot is known about the electrochemical and surface⁴ properties of mesoporous and nanoparticulate TiO₂.^{5–8} Models have been developed⁹ to describe the capacitive and reactive properties of nanoporous semiconducting TiO₂. TiO₂ is an important material in electrochemistry,¹⁰ photochemistry¹¹ and for sensor systems.¹² In combination with other more electrically conducting transition metal oxides, TiO₂ is employed in dimensionally stable anodes¹³ and in a hydrogen-reduced electrically conducting form in EbonexTM electrodes.¹⁴ Composites of TiO₂ and carbon have been employed to combine the surface reactivity of TiO₂ and the electrical conductivity of graphite.¹⁵

In this study the core-shell nanostructure approach is applied to TiO₂ systems. Incorporation of a second component with TiO₂ to form core-shell structures has attracted considerable recent interest with a variety of applications in catalysis. These include TiO₂–BaFe₁₂O₁₉ core-shell nanoparticles for improving photo-catalysis¹⁶ and the use of TiO₂–Ag core-shell structures for catalysis with improved electronic transportation.¹⁷ Other studies describe the use of TiO₂–silica core-shell colloidal particles for optical trapping applications¹⁸ and the use of TiO₂ coated polystyrene core-shell spheres for electronic ink applications.¹⁹

TiO₂ behaves like an insulator over a wide range of positive potentials.²⁰ It is shown here that by introducing the TiC core, it is possible to increase conductivity whilst maintaining an active TiO₂ surface. Micron-scale core-shell composites of TiO₂ and TiC have been formed recently through controlled thermal plasma oxidation.²¹ TEM observations of oxide scale formed on TiC single crystals with different faces has been reported using thermal oxidation.²² Reducing the size of the TiC particles to nanoparticles can provide an exceptionally high surface area for adsorption and electrocatalysis. TiO₂ is a biocompatible substrate material for the adsorption of proteins and small redox active molecules.²³

The voltammetric detection of small biologically important molecules such as ascorbic acid or quinols such as hydroquinone and dopamine is of considerable interest and these systems are employed here as model systems. For these redox systems a variety of methods has been developed, for example electrochemical detection after separation in capillary electrophoresis,²⁴ or the use of modified electrodes with polyaniline²⁵ or graphite reinforced by carbon.²⁶ In voltammetric

^a Department of Chemistry, Loughborough University, Loughborough, Leicestershire, UK LE113TU

^b Division of Research Initiatives, International Innovation Centre, Kyoto University, Nishikyo-ku, Kyoto, 615-8520, Japan

^c Department of Chemistry, University of Bath, Claverton Down, Bath, UK BA2 7AY. E-mail: F.Marken@bath.ac.uk

measurements of extra cellular fluid, ascorbic acid is reported as being the main interfering molecule with dopamine.²⁷ Depending on the conditions of the experiment, the surface charge of the TiO₂ may help separating the responses for the negatively charged ascorbic acid and the positively charged dopamine. The electrocatalytic behavior for the oxidation of hydroquinone, dopamine and ascorbic acid using core-shell TiC–TiO₂ nanoparticle films on ITO electrode surfaces is surveyed.

2. Experimental

2.1. Chemical reagents

K₂HPO₄, KH₂PO₄, methanol, L-ascorbic acid, dopamine and hydroquinone were obtained commercially and used without further purification. TiC nanoparticles (20–30 nm diameter) were obtained as dry powder from Goodfellow, UK. Demineralised water was obtained from an Elgastat purification system (Elga, High Wycombe, Bucks, UK) with a resistivity not less than 18 MΩ cm.

2.2. Instrumentation

Electrochemical experiments were conducted with an Autolab system (Eco Chemie, NL) in a three electrode cell. The reference and counter electrodes were saturated calomel (SCE) and platinum foil, respectively. The porous TiC working electrodes were prepared from ITO coated glass (active area 10 mm × 10 mm, resistivity 20 Ω per square) obtained from Image Optics Components Ltd (Basildon, Essex, UK). An Elite tube furnace system was used for cleaning ITO electrode surfaces (at 500 °C in air) and for thermally oxidizing metal carbide films in air. Prior to electrochemical experiments, solutions were de-aerated with high purity argon (BOC, UK). Quartz crystal microbalance experiments were conducted with ITO-coated quartz crystals (Part no. QA-A-9M-ITOM, Advanced Measurement Technology, Wokingham, Berks, UK). A quartz crystal oscillator circuit (Oxford Electrodes) connected to a frequency counter (Fluke, PM6680B) allowed the resonance frequency of the quartz crystal sensor to be monitored. The 9.1 MHz AT-cut quartz crystal microbalance system was calculated²⁸ to have a sensitivity factor of $\Delta m/\Delta f = -1.05 \text{ ng Hz}^{-1}$ in air based on the expression

$$\frac{\Delta m}{\Delta f} = -\frac{A \times \sqrt{\mu_Q \rho_Q}}{2f_0^2}$$

with the area $A = 0.2 \text{ cm}^2$, the resonance frequency $f_0 = 9.1 \times 10^6 \text{ Hz}$, the density of quartz $\rho_Q = 2.648 \text{ g cm}^{-3}$, and the shear modulus of quartz $\mu_Q = 2.947 \times 10^{11} \text{ g cm}^{-1} \text{ s}^2$. Field emission gun scanning electron microscopy (FEGSEM) images were obtained using a Leo 1530 Field Emission Gun SEM system. Transmission electron microscopy (TEM) images were obtained using a JEM-2000FX electron microscope. All experiments were conducted at $22 \pm 2 \text{ °C}$ except high temperature XRD measurements. The XRD measurements were performed on a Bruker D8 diffractometer fitted with primary monochromator using Cu Kα1 radiation and an Anton Parr HTK 1200 heated sample stage. The sample was

heated at 2 °C min^{-1} and held at each temperature for 30 min before data were collected between $20\text{--}80^\circ 2\theta$ using a $0.0147^\circ 2\theta$ step over a period of 30 min.

2.3. Stepwise deposition of TiC nanoparticle films

For experiments using ITO glass electrodes, mesoporous films of TiC were deposited following a repeated deposition coating method. A clean ITO surface (washed with ethanol and water, dried, and 30 min heat treatment at 500 °C in air) was dipped into a suspension of TiC nanoparticles in methanol (*ca.* 0.03 g TiC in 10 cm³ methanol, dispersed by ultrasonication). After 30 s the ITO electrode was removed and the methanol allowed to evaporate in air at room temperature. This leaves a permanently adhered film of TiC particles on the ITO electrode surface. By repeatedly dipping the resulting nanoparticle modified electrode into the TiC suspension, more thicker deposits of TiC were produced on the ITO surface. The electron microscopy images shown in Fig. 1A show spherical nanoparticles of *ca.* 20–30 nm diameter aggregated and deposited randomly and non-uniformly on the electrode surface.

3. Results and discussion

3.1. Deposition and characterisation of TiC nanoparticle films on ITO

TiC nanoparticles are readily deposited from a suspension in methanol onto ceramic electrode surfaces such as ITO coated glass. The deposition can be repeated allowing a thin film to form with increasing thickness depending on the number of deposition cycles. Typical scanning electron microscopy images of a ‘five-layer’ deposit are shown in Fig. 1A. It can be seen that the typical particle size is 20–30 nm and that

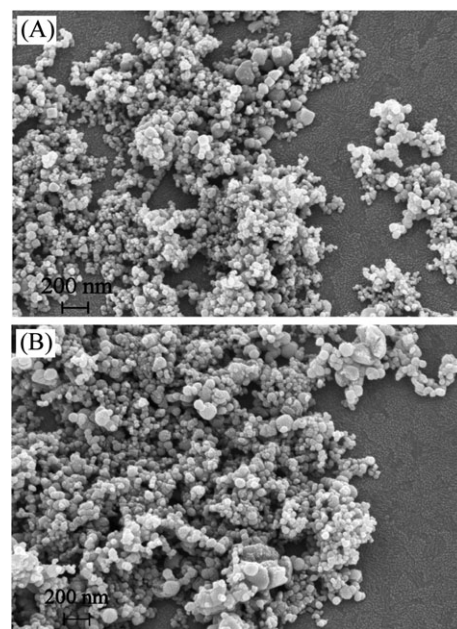


Fig. 1 FEGSEM images for (A) TiC nanoparticles (5 layers, *ca.* 20–30 nm diameter) deposited on ITO and (B) a similar film of TiO₂ nanoparticles obtained by heat treatment of TiC nanoparticles (500 °C in air for 30 min).

agglomerates of particles dominate the non-uniform deposit. The repeated deposition results in growth of a patchy, porous film on the electrode surface. A key factor in the slow growth rate is the low concentration of TiC nanoparticles (0.3 wt% in methanol). This allows stepwise control of the amount of deposit and the average film thickness.

The electron microscopy data are supported by experiments with a quartz crystal microbalance system. Fig. 2A shows the reduction of the resonance frequency of an ITO coated quartz crystal resonator during the repeated deposition process. Each deposition reduces the resonance frequency by approximately 1230 Hz which corresponds to 1.29 μg (according to the Sauerbrey equation,²⁹ see Experimental). The weight of TiC deposit (molecular weight 59.91 g mol^{-1}) can be converted into the estimated amount 2.2×10^{-8} mol per layer (on a 0.2 cm^2 area of the quartz resonator).

Next, the TiC nanoparticle films were characterized electrochemically after immersion in 0.1 M phosphate buffer solution pH 7. Voltammetric experiments were conducted over a wide potential window with 3 new processes observed compared to data obtained at a clean ITO electrode (see Fig. 2B). Firstly, a

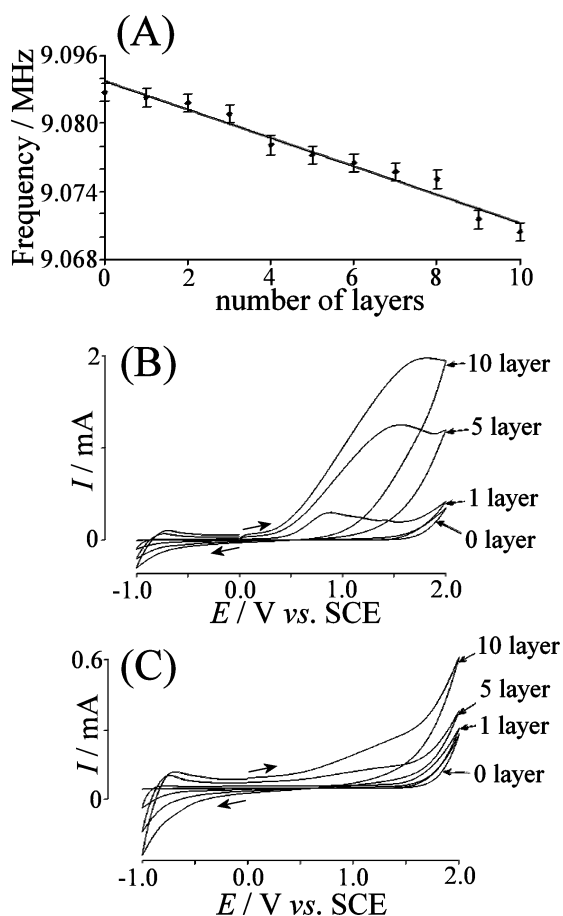


Fig. 2 (A) Plot of the resonance frequency change for an ITO coated quartz crystal during repeated deposition of TiC. The frequency change corresponds to a mass increase with 1.05 ng Hz^{-1} (see experimental). (B,C) Cyclic voltammograms (scan rate 50 mV s^{-1}) obtained for (B) scan 1 and (C) scan 2 of the irreversible surface oxidation of TiC films with increasing thicknesses immersed in aqueous 0.1 M phosphate buffer pH 7.

large irreversible anodic electrochemical response at a potential of 1 V vs. SCE is generated. The current for this oxidation is directly proportional to the average TiC film thickness (or the amount of TiC deposited). This anodic response is dominating during the first potential cycle and can be attributed to a possible surface reaction which is resulting in carbon oxidation and formation of hydrolyzed titanium oxide film (eqn (1)).



The charge under the anodic response during the first potential cycle, *ca.* 6 mC for a one layer deposit, is consistent with approximately 10^{-8} mol or 10% of the TiC deposit. It can be proposed that a surface oxidation occurs and a thin film of TiO_2 is formed around the TiC particles.

The second notable feature is a capacitive background current that is again proportional with the average thickness of TiC film. Thirdly, it is possible to observe a redox response at a potential of *ca.* -0.8 V vs. SCE . The shape of this voltammetric response is characteristic for TiO_2 thin films and has been explained in terms of sequential filling electronic states within the oxide.⁹ By initially scanning to more negative potentials prior to the electrochemical oxidation of the TiC, the change in redox response associated with the formation of the titania film becomes more apparent, confirming the process shown in eqn (1) (data not shown).

In order to determine whether a “visible” shell of titanium oxide was formed on the TiC nanoparticle surface after electrochemical oxidation, TEM images were obtained. The image shown in Fig. 3A confirms that an amorphous shell, approximately 2 nm in thickness, is indeed formed upon electrochemical oxidation on the surface of the TiC nanoparticles. From this image it appears as if most particles are affected by the surface oxidation but it is difficult to judge the uniformity of the conversion. The resulting particles are suggested to have “core-shell” nature based on the symmetric coating of particles with an oxide layer.

3.2. Thermal oxidation of titanium carbide nanoparticles to TiC– TiO_2 core-shell nanoparticles

As a second approach for the formation of TiO_2 surface layers thermal oxidation in air was investigated. When heated in air at $500 \text{ }^\circ\text{C}$, the black TiC nanoparticles were converted into a white nanoparticulate material. The FEGSEM images of this material show no dramatic change in appearance before and after thermal treatment (see Fig. 1). However, an increase in volume is expected. Based on the volume per formula unit (room temperature densities are for anatase = 3.895 g cm^{-3} and for TiC = 4.93 g cm^{-3}) which is 20.3 \AA^3 for TiC and 34.1 \AA^3 for TiO_2 an increase in volume by 69% is expected (increase in radius *ca.* 19%).

To further quantify this process and to confirm the identity of the white nanoparticles, TiC nanoparticles were gradually thermally oxidized in air under XRD conditions (see Fig. 4).

The XRD line pattern for TiC, TiO_2 (anatase), and TiO_2 (rutile) can be clearly identified. At $300 \text{ }^\circ\text{C}$ the TiC phase is seen to be reacting and at $350 \text{ }^\circ\text{C}$ oxidation to the anatase form of TiO_2 has occurred. A grey intermediate product is obtained at $300 \text{ }^\circ\text{C}$. This intermediate product shows a core-shell

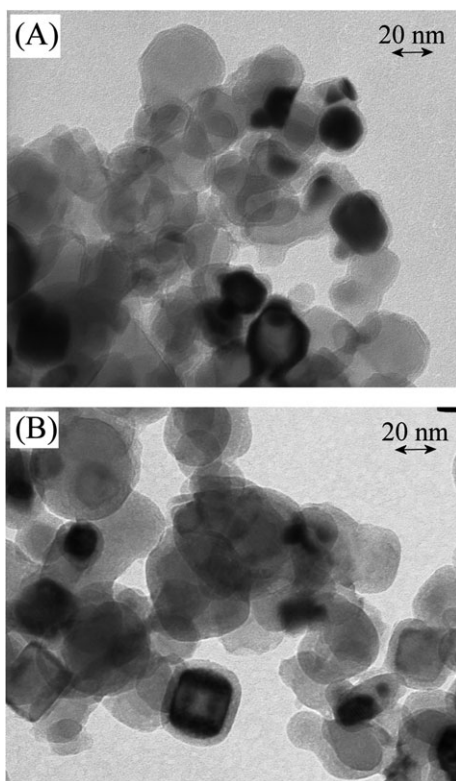
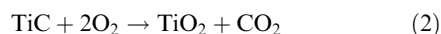


Fig. 3 (A) TEM image of core-shell titanium carbide–titanium oxide nanoparticles formed after the irreversible surface oxidation (+2 V vs. SCE applied for 60 s) of TiC nanoparticles in aqueous 0.1 M phosphate buffer pH 7. (B) TEM image of core-shell titanium carbide–titanium oxide nanoparticles after the thermal surface oxidation of TiC nanoparticles at 300 °C for 30 min in air.

structure when investigated by TEM (see Fig. 3B). At temperatures greater than 700 °C, the crystal structure of the rutile form of TiO₂ starts to appear. Fig. 4B shows a plot of the percentage phase composition with gradual thermal oxidation in air. The transition from TiC to anatase occurs rapidly over a 50 °C range compared to the more gradual transition from anatase to rutile at higher temperature. A possible reaction for the surface oxidation of TiC is proposed in eqn (2).



The Scherrer equation, $t = \frac{0.9\lambda}{\sqrt{B_m^2 - B_s^2} \cos \theta}$ (t = average crystallite size in Å, B_m and B_s = width in radians of the diffraction peaks at half maximum height of the test sample and a highly crystalline standard (0.1°) sample, respectively, and λ = wavelength of the X-ray beam in Å) relates the average size of a crystal grain to the width of its diffraction peaks. As a result it is possible to show that the average particle or grain sizes of the TiC are very similar before (approximately 30 nm) and after thermal oxidation at 500 °C (approximately 28 nm). This result is consistent with the electron microscopy observations (see Fig. 1).

Next, the voltammetric characteristics of thermally oxidized TiC nanoparticle films are investigated. The effect of thermal oxidation on the background electrochemical properties of TiC films was investigated in 0.1 M phosphate buffer solution

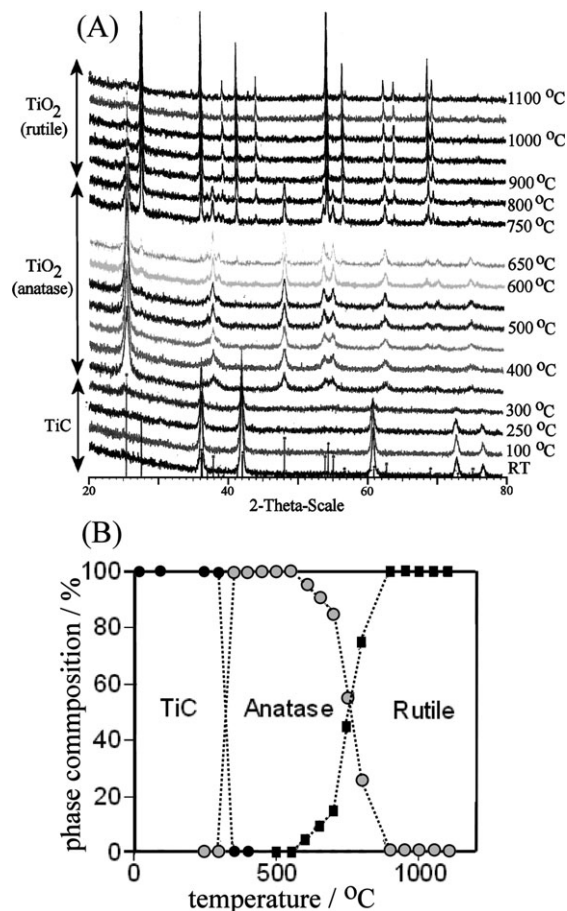


Fig. 4 (A) Plot of XRD data for the gradual thermal oxidation of TiC to TiO₂ (anatase) at 350 °C and to TiO₂ (rutile) at temperatures higher than 700 °C. The sample was heated in 50 °C intervals per 30 min. (B) Plot of percent phase composition during gradual thermal oxidation of TiC in air under XRD conditions.

pH 7 as before. Fig. 5 shows the cyclic voltammograms for the first and second scans for a ‘10-layer’ TiC film with no prior thermal oxidation and a ‘10-layer’ partially oxidized TiC–anatase core-shell film produced after 30 min thermal oxidation of a TiC film at 300 °C. Data for a ‘10-layer’ anatase film produced after 30 min thermal oxidation of a TiC film at 500 °C are also shown.

The partially oxidized TiC–TiO₂ core-shell nanoparticle film demonstrates a large decrease in the electrochemical surface oxidation and slight decrease in background capacitive current compared to the TiC film. An increase in the Ti(IV/III) redox response at negative potentials is also seen. This is as expected due to the decrease in size of the highly conductive TiC core and increase in the amount of surface TiO₂ prior to the electrochemical experiments. The anatase film shows background capacitive currents similar to a clean ITO electrode and no surface TiC oxidation. The Ti(IV/III) redox response is similar for the fully and the partially oxidized TiC–TiO₂ core-shell nanoparticles. These results clearly show that electrochemical and thermal oxidation result in similarly behaved core-shell structures. Next, the electrochemical properties for some model redox systems at TiC–TiO₂ core-shell nanoparticle modified electrodes are investigated.

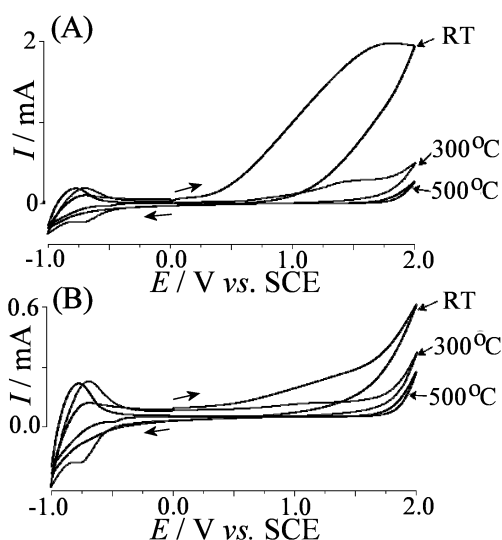
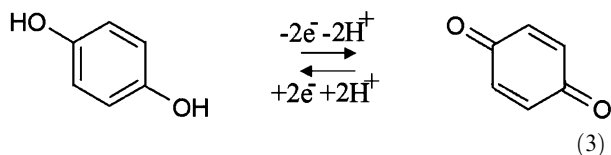


Fig. 5 Cyclic voltammograms (scan rate 50 mV s^{-1}) obtained for (A) scan 1 and (B) scan 2 of the irreversible surface oxidation of TiC films after thermal oxidation in aqueous 0.1 M phosphate buffer pH 7.

3.3. The electrocatalytic oxidation of hydroquinone on nanoparticulate titanium carbide

It has been demonstrated recently that bulk TiC is an attractive electrode material for electroanalytical processes and that in particular quinone systems show fast electron transfer.³ Here, the effect of TiC nanoparticles on electrochemical processes is surveyed for comparison. The electrochemical oxidation of 2 mM hydroquinone in 0.1 M phosphate buffer pH 7 with new TiC films is shown in Fig. 6 (eqn (3)).



For the oxidation of hydroquinone using only a clean ITO electrode, a peak-to-peak separation of 2.26 V is observed as a large overpotential is necessary before oxidation and reduction are possible on clean ITO. In contrast, in the first scan using a porous ‘5-layer’ TiC film, a much more reversible process (peak separation of 0.89 V) is produced. Increasing the amount of TiC further decreases the peak-to-peak separation to 0.61 V (see Fig. 6A).

The electrochemical surface oxidation of TiC is seen in the first oxidation cycle as before. Interestingly, the hydroquinone oxidation and re-reduction responses are not affected by the formation of the TiC–TiO₂ core-shell structure (see Fig. 6B). The interaction of the surface with the hydroquinone as well as the electrical conductivity appear to be very effective. The reactivity towards hydroquinone remains high even after cycling to $+2 \text{ V}$. The shape of the voltammogram for the oxidation and reduction of hydroquinone is consistent with that reported in the literature.³

For TiC films with only ‘1-layer’, a much lower loading of TiC is achieved. Fig. 6C shows the oxidation and reduction of 2 mM hydroquinone using a very thin TiC film electrode at

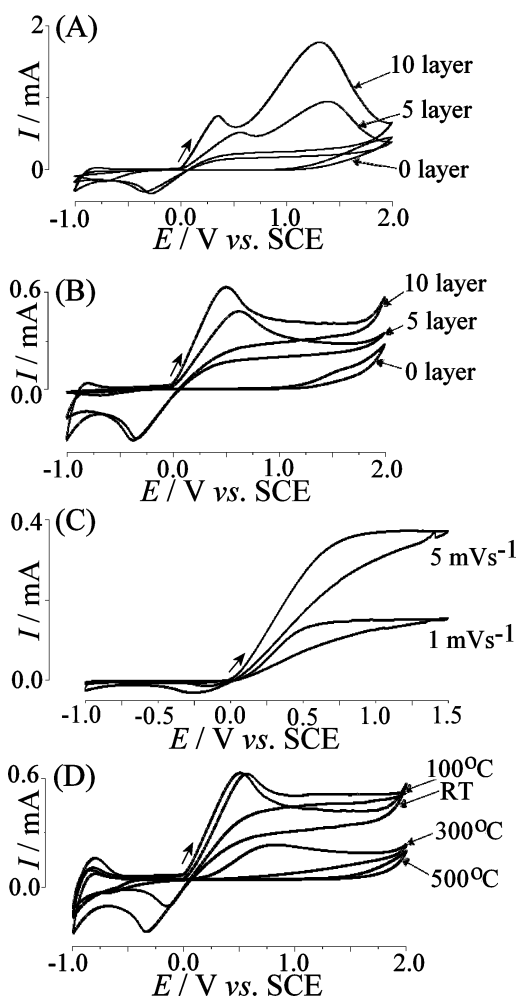


Fig. 6 (A,B) Cyclic voltammograms (scan rate 50 mV s^{-1}) obtained for (A) scan 1 and (B) scan 2 of the irreversible surface oxidation of TiC films with increasing thicknesses in aqueous 0.1 M phosphate buffer pH 7 in the presence of 2 mM hydroquinone. (C) Cyclic voltammograms (scan 2 shown, scan rates 5 mV s^{-1} and 1 mV s^{-1}) obtained for the oxidation of 2 mM hydroquinone using a 1 layer TiC film in aqueous 0.1 M phosphate buffer pH 7. (D) Cyclic voltammograms (scan rate 50 mV s^{-1}) obtained for the oxidation of 2 mM hydroquinone at TiC films after thermal oxidation (scan 2 for RT; scan 1 for heat treated electrodes) immersed in aqueous 0.1 M phosphate buffer pH 7.

slower scan rates. The same type of almost sigmoidal voltammetric response is seen at 50 mV s^{-1} (not shown). The dependence of the sigmoidal voltammogram on scan rate indicates that a micro array of TiC nanoparticle aggregates is present and overlapping diffusion zones are responsible for the shape.

Next, the effect of TiC thermal oxidation on the electrocatalytic oxidation of hydroquinone was also investigated. Using a ‘10-layer’ TiC film heat treated at increasing temperatures, it is shown that as the TiC film is gradually oxidized, the electrocatalytic nature of the film decreases (see Fig. 6D). The treatment at $300 \text{ }^\circ\text{C}$ clearly reduces the electrocatalytic effect (peak-to-peak separation) and the magnitude of the current but a well defined response is still observed. Only after complete conversion to TiO₂ (anatase) is the signal for the

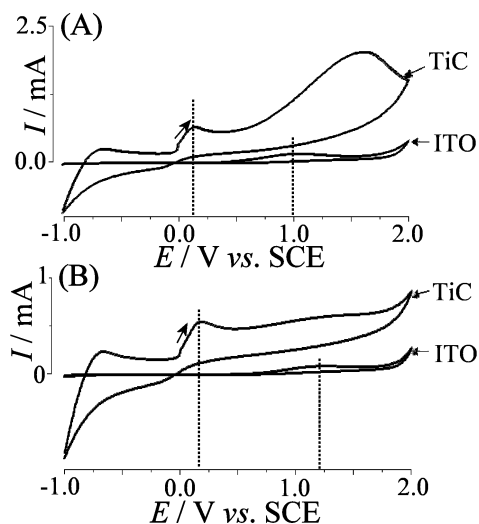
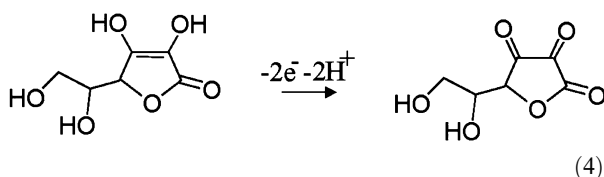


Fig. 7 Cyclic voltammograms (scan rate 50 mV s^{-1}) obtained for (A) scan 1 and (B) scan 2 of the irreversible surface oxidation of a 10 layer TiC film and clean ITO in aqueous 0.1 M phosphate buffer pH 7 in the presence of 2 mM ascorbic acid.

hydroquinone oxidation lost. This indicates (i) a need for the highly conductive TiC core and (ii) that even with a substantial TiO_2 shell a high level of electrocatalytic reactivity can be maintained.

3.4. The electrocatalytic oxidation of ascorbic acid on nanoparticulate titanium carbide

The electrocatalytic oxidation of 2 mM ascorbic acid was investigated in 0.1 M phosphate buffer solution at pH 7 using a '10-layer' TiC film electrode and compared to data obtained with a clean ITO (see Fig. 7). The process is assumed to be 2-electron in nature (eqn (4)) and chemically irreversible due to follow-up hydration processes.



For both electrodes, a single irreversible oxidation peak is produced, consistent with experiments carried out with other modified electrodes.²⁷ As for the oxidation of hydroquinone, the greater conductivity and reactivity of TiC results in the oxidation for ascorbic acid at lower potentials. After surface oxidation of the TiC in scan 1, electrocatalysis for ascorbic acid oxidation is still maintained in scan 2. Substantial oxidation of ascorbic acid occurs at potentials of *ca.* 0 V vs. SCE and the magnitude of the current is proportional to ascorbic acid concentration.

3.5. The electrocatalytic oxidation of dopamine on nanoparticulate titanium carbide

A similar experiment was carried out in the presence of 2 mM dopamine and 2 broad oxidation and reduction peaks are observed in the absence of TiC (see Fig. 8). The oxidation and

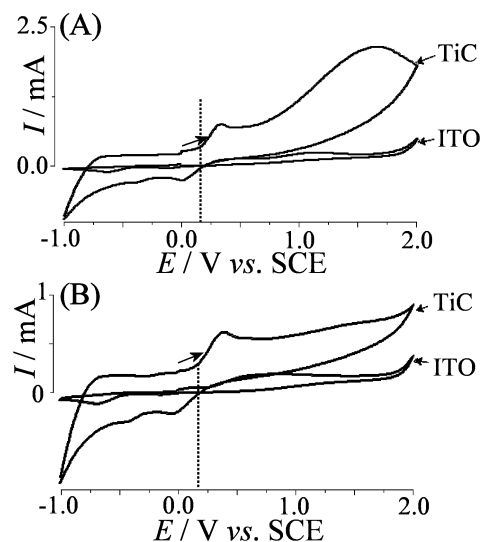
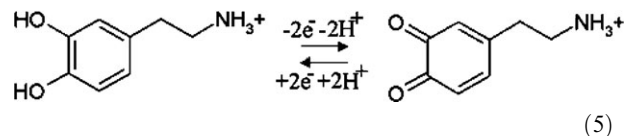


Fig. 8 Cyclic voltammograms (scan rate 50 mV s^{-1}) obtained for (A) scan 1 and (B) scan 2 of the irreversible surface oxidation of a 10 layer TiC film and clean ITO in aqueous 0.1 M phosphate buffer pH 7 in the presence of 2 mM dopamine.

re-reduction of dopamine (see eqn (5)) at clean ITO was highly irreversible and in the presence of TiC nanoparticles almost reversible responses (consistent with previous studies²⁷) are observed.



The oxidation of dopamine occurs with a peak current proportional to dopamine concentration and at a potential approximately 0.1 V more positive compared to the oxidation of ascorbic acid under the same conditions.

The reactivity of TiC– TiO_2 core-shell nanoparticles has been surveyed only in aqueous phosphate buffer media here. However, the reactivity of the surface can be expected to change depending on the availability of surface sites and the ability of the analyte to reversibly bind to the surface. Further improvements in selectivity towards analytes will be possible in future.

4. Conclusions

It has been shown that TiC nanoparticles can be electrochemically and thermally oxidized to give what appear to be core-shell TiC– TiO_2 nanoparticles. The shape and appearance of the particles are not affected by the solid state transformation from TiC to TiO_2 and the oxide film appears to grow symmetrically around the particles. However, the electrical properties change from those of a good conductor to a semiconductor. Core-shell TiC– TiO_2 nanoparticles represent a novel electro-catalytically active material for mesoporous thin films or other types of composite electrodes *e.g.* pastes. Catalytic effects have been demonstrated for oxidation of hydroquinone, dopamine, and ascorbic acid. TiO_2 shells

provide adsorption sites and well defined surface properties whereas TiC cores provide conductivity over a wide potential window.

Acknowledgements

S. J. S. thanks the RSC and the EPSRC for an Analytical Science Studentship. We thank Mr J. S. Bates for his help with the FEGSEM and TEM measurements.

References

- 1 G. Radhakrishnan, R. E. Robertson, P. M. Adams and R. C. Cole, *Thin Solid Films*, 2002, **420–421**, 553.
- 2 W. Lu, D. Zhang, R. Wu, T. Sakata and H. Mori, *J. Alloys Compd.*, 2001, **327**, 248.
- 3 A. Lupu, D. Compagnone, S. Orlanducci, M. L. Terranova, V. Magearu and G. Palleshi, *Electroanalysis*, 2004, **16**, 1704.
- 4 U. Diebold, *Surf. Sci. Rep.*, 2003, **48**, 53.
- 5 L. Kavan, M. Grätzel, J. Rathousky and A. Zukal, *J. Electrochem. Soc.*, 1996, **143**, 394.
- 6 G. Boschloo and D. Fitzmaurice, *J. Electrochem. Soc.*, 2001, **147**, 1117.
- 7 J. Bisquert, *J. Phys. Chem. B*, 2004, **108**, 2323.
- 8 I. Mora-Sero and J. Bisquert, *Nano Lett.*, 2003, **3**, 945.
- 9 F. Fabregat-Santiago, I. Mora-Sero, G. Garcia-Belmonte and J. Bisquert, *J. Phys. Chem. B*, 2003, **107**, 758.
- 10 K. J. McKenzie, P. M. King, F. Marken, C. E. Gardner and J. V. Macpherson, *J. Electroanal. Chem.*, 2005, **579**, 267.
- 11 N. S. Allen, M. Edge, G. Sandoval, J. Verran, J. Stratton and J. Maltby, *Photochem. Photobiol.*, 2005, **81**, 279.
- 12 P. K. Dutta, M. Frank, G. W. Hunter and M. George, *Sens. Actuators, B*, 2005, **106**, 810.
- 13 S. Trasatti, *Electrochim. Acta*, 2000, **45**, 2377.
- 14 P. C. S. Hayfield, *Development of a New Electrode Material Monolithic Ti₄O₇ Ebonex Ceramic*, Finishing Publication Ltd, Stevenage, UK, 2002.
- 15 Y. Wang, C. Li and S. Hu, *J. Solid State Electrochem.*, 2006, **10**, 383.
- 16 W. Y. Fu, H. B. Yang, M. H. Li, L. X. Chang, Q. J. Yu, J. Xu and G. T. Zou, *Mater. Lett.*, 2006, **60**, 2723.
- 17 I. Pastoriza-Santos, D. S. Koktysh, A. A. Mamedov, M. Giersig, N. A. Kotov and L. M. Liz-Marzan, *Langmuir*, 2000, **16**, 301.
- 18 P. Viravathana and D. W. M. Marr, *J. Colloid Interface Sci.*, 2000, **221**, 301.
- 19 I. B. Jang, J. H. Sung, H. J. Choi and I. Chin, *Synth. Met.*, 2005, **152**, 9.
- 20 E. V. Milsom, H. R. Perrott, L. M. Peter and F. Marken, *Langmuir*, 2005, **21**, 9482.
- 21 Y.-L. Li and T. Ishigaki, *Chem. Phys. Lett.*, 2003, **367**, 561.
- 22 H. Kiyono, S. Shimada, K. Sugawara and A. Christensen, *Solid State Ionics*, 2003, **160**, 373.
- 23 K. J. McKenzie, F. Marken and M. Opallo, *Bioelectrochem.*, 2005, **66**, 41.
- 24 W. R. Vandaveer IV, S. A. Pasas-Farmer, D. J. Fischer, C. N. Frankenfeld and S. M. Lunte, *Electrophoresis*, 2004, **25**, 3528.
- 25 V. Zucolotto, M. Ferreira, M. R. Cordeiro, C. J. L. Constantino, W. C. Moreira and O. N. Oliveira, Jr, *Sens. Actuators, B*, 2006, **113**, 809.
- 26 K. Miyazaki, G. Matsumoto, M. Yamada, S. Yasui and H. Kaneko, *Electrochim. Acta*, 1999, **44**, 3809.
- 27 S.-M. Chen and W.-Y. Chzo, *J. Electroanal. Chem.*, 2006, **587**, 226.
- 28 M. D. Ward, in *Physical Electrochemistry*, ed. I. Rubinstein, Marcel Dekker, New York, 1995, p. 297.
- 29 M. D. Ward, in *Physical Electrochemistry*, ed. I. Rubinstein, Marcel Dekker, New York, 1995, p. 293.